

## WALL-ATTACHED MOMENTUM TRANSFER STRUCTURES IN SLIP CHANNEL FLOWS

**Junwoo Jae**

School of Mechanical Engineering  
Pusan National University  
Busan 46241, Korea  
jjw8557@pusan.ac.kr

**Hyung Jin Sung**

Department of Mechanical Engineering  
KAIST  
Daejeon 34141, Korea  
hjsung@kaist.ac.kr

**Jinyul Hwang**

School of Mechanical Engineering  
Pusan National University  
Busan 46241, Korea  
jhwang@pusan.ac.kr

### ABSTRACT

Reducing skin-friction drag in wall turbulence is crucial for minimizing energy consumption in various industrial applications. Although numerous studies have proposed strategies for the skin-friction reduction, their effectiveness primarily degrades at high Reynolds numbers ( $Re$ ) encountered in many practical flows. To achieve skin-friction reduction in high-Reynolds-number flows, characterized by multiscale phenomena, a detailed understanding of coherent structures, which span a wide range of scales, is necessary, especially regarding structures that extend to the wall. In the present work, we explore the wall-attached momentum transfer structures ( $Qs$ ) in drag-reduced flows and the associated  $Re$  effects on the skin-friction reduction. By employing the Navier slip boundary conditions, we obtain the drag-reduced flows at two bulk  $Re$  of 10,000 and 20,000. For comparison, we conduct the no-slip cases at the same bulk  $Re$ . We observe that wall-attached  $Qs$  play a dominant role in both skin-friction generation and reduction. These structures are classified into the buffer-layer, self-similar, and non-self-similar ones according to their height. The self-similar structures exhibit self-similarity in both size and Reynolds shear stress, and these remain unaffected under slip conditions. Due to their self-similarity, the self-similar structures show nearly identical skin-friction reduction across all heights. In contrast, the non-self-similar structures exhibit a significant difference under slip conditions. Particularly at a high  $Re$ , the volume reduction of non-self-similar structures and the decrease in the associated wall-normal transport under slip conditions result in greater skin-friction reduction compared to a low  $Re$ . Our findings advance the understanding of wall-attached structures' scale-dependent behaviour in drag-reduced flows, paving the way for developing new drag reduction methods by strategic manipulation of these structures.

### INTRODUCTION

Wall turbulence is a prevalent phenomenon in natural environments and engineering applications. Due to the presence of the wall, a strong shear layer forms near the wall, which is the source of most of drag. In terms of energy consumption, reducing skin-friction drag is a major topic in various industrial applications, such as pipelines, airplanes, and ships. Over a long period, numerous studies have introduced drag reduction strategies, either through passive or active means (Kasagi et al., 2009; Kim, 2011). However, most practical flows are of a high Reynolds number ( $Re$ ), which

makes many of these drag-reduction strategies less effective. In particular, at these high-Reynolds-number flows, multiscale phenomena become more pronounced. Without a comprehensive understanding of the wide range of scales present within wall-bounded turbulent flows, developing an effective drag reduction scheme at high  $Re$  is challenging.

One way to understand the multiscale phenomena in wall turbulence is through the investigation of coherent structures (Robinson, 1991; Adrian, 2007). In this context, it is essential to analyse turbulent coherent structures and their interactions from the perspective of skin-friction generation to develop a new skin-friction scheme (Yoon et al., 2016a; Hwang & Sung, 2017; Yoon et al., 2018). In the near-wall region, two dominant coherent structures—low-speed streaks and quasi-streamwise vortices—play a significant role in a self-sustaining cycle (Hamilton et al., 1995). Low-speed streaks undergo a process known as bursting, which includes lift-up, oscillation, break-up, and ejection (Kline et al., 1967). This bursting process can be characterized by the quadrant analysis introduced by Wallace et al. (1972) and Willmarth & Lu (1972). Instantaneous Reynolds shear stress ( $uv$ ) is categorized based on the streamwise and wall-normal velocity fluctuations ( $u$  and  $v$ ) into four quadrants: Q1 ( $u > 0, v > 0$ ), Q2 ( $u < 0, v > 0$ ), Q3 ( $u < 0, v < 0$ ), and Q4 ( $u > 0, v < 0$ ). Lu & Willmarth (1973) demonstrated that the Q2 and Q4 structures, referred to as momentum transfer structures ( $Qs$ ), dominantly contribute to the total Reynolds shear stress (RSS) in turbulent boundary layers. In addition, these  $Qs$  are directly associated with the turbulent production, which, in turn, contributes to skin-friction generation (Kim, 2011).

Beyond the near-wall region, coherent structures characterized by an outer length scale—such as large-scale and very-large-scale motions—have been observed in the logarithmic and outer regions (Kovaszny et al., 1970; Kim & Adrian, 1999; Hwang et al., 2016a; Han et al., 2019; Hwang & Lee, 2022). These structures extend down to the near-wall region and influence the near-wall coherent structures and the wall-shear stress (Hutchins & Marusic, 2007; Hwang et al., 2016b; Hwang & Sung, 2017). Additionally, in the log region, self-similar coherent structures whose sizes are proportional to wall-normal distance ( $y$ ) exist at high-Reynolds-number flows (Townsend, 1961). Moreover, even at moderate  $Re$ , the existence of self-similar structures has been found in canonical wall turbulence (Hwang & Sung, 2018, 2019; Hwang et al., 2020). These self-similar energy-containing motions are vital

for generating skin friction and their importance increases with  $Re$  (de Giovanetti et al., 2016).

Numerous studies have observed the modulation of coherent structures within drag-reduced flows. A passive control method for drag reduction involves the use of hydrophobic surfaces (Tretheway & Meinhart, 2002). Min & Kim (2004) conducted direct numerical simulations (DNSs) of turbulent channel flows with a slip boundary condition at walls to model the hydrophobic surface. They confirmed that the presence of weakened streamwise vortices in the near-wall region and a reduced mean shear contribute to drag reduction under streamwise slip conditions. Yoon et al. (2016b) studied the relationship between large-scale motions and drag reduction in a slip channel flow. They found that the wall-parallel sizes of outer negative- $u$  structures increase, alongside an increase in their footprint area. As a result, these changes lead to a decrease in the total skin friction, because the negative  $u$  attenuates the small scales in the near-wall region. Recently, Yoon & Sung (2022) reported similar findings by focusing on wall-attached  $u$  structures. However, there is still a need to elucidate the contributions of coherent structures and their associated multiscale characteristics at higher  $Re$ .

The object of the present study is to explore the contributions of wall-attached Qs to turbulent skin friction in drag-reduced flows by focusing on the associated  $Re$  effect. To this end, we performed DNSs of fully-developed turbulent channel flows at bulk  $Re$  of 10,000 and 20,000 under slip boundary conditions and compared them with the DNS data obtained under no-slip boundary conditions. Wall-attached Qs are extracted from the instantaneous flow fields, and their contributions to skin-friction generation and its reduction are analysed using FIK identity (Fukagata et al., 2002). Wall-attached Qs are decomposed into the buffer-layer, self-similar, and non-self-similar ones according to their height. We then explore the behaviours of each structure under slip conditions and how these behaviours vary with  $Re$ .

## NUMERICAL DETAILS

In this study, we performed the DNSs of fully-developed turbulent channel flows under slip and no-slip conditions. The fractional step method proposed by Kim et al. (2002) was used to solve the Navier–Stokes equations and the continuity equation for an incompressible flow. The streamwise and spanwise domain sizes were set to  $L_x = 2\pi\delta$  and  $L_z = \pi\delta$ , respectively, where  $\delta$  indicates the channel half-height. These domain sizes are found to be enough to obtain the correct one-point turbulence statistics across the turbulence channel flow (Lozano-Durán & Jiménez, 2014). The periodic boundary conditions were applied in the streamwise and spanwise directions. To simulate the drag-reduced flow, we applied the Navier slip boundary condition to both walls. This condition was used to mimic a hydrophobic surface in previous studies (Min & Kim, 2004; Yoon et al., 2016b). The streamwise velocity at the wall was imposed as follows:

$$U_s = L_s (dU / dy)|_{wall} \quad (1)$$

where  $U_s$  and  $L_s$  are the slip velocity length, respectively. We set the slip length of  $0.01\delta$  (Yoon et al., 2016b). The simulations were conducted at two bulk Reynolds numbers ( $Re_b = U_b\delta/\nu$ ) of 10,000 and 20,000 where  $U_b$  indicates the bulk velocity and  $\nu$  denotes the kinematic viscosity. Throughout this paper, NL and SL denote the no-slip and slip cases at a low  $Re_b$ ,

respectively, whereas NH and SH indicate those at a high  $Re_b$ . In all the DNSs, a constant mass-flow rate was maintained. Hence, the  $Re_b$  for both no-slip and slip cases remains the same, but the friction Reynolds number ( $Re_\tau = u_\tau\delta/\nu$ ) for the slip cases is lower than that for the no-slip cases. The friction Reynolds numbers corresponding to each case are as follows:  $Re_\tau = 538$  for NL, 443 for SL, 992 for NH, and 743 for SH. The drag reduction rate is 33% and 44% for the low and high  $Re$ , respectively. The streamwise, wall-normal, and spanwise directions are denoted as  $x$ ,  $y$ , and  $z$ , respectively, and  $U$ ,  $V$ , and  $W$  represent the corresponding velocity components. An angle bracket  $\langle \cdot \rangle$  indicates mean quantities, which are temporally and spatially averaged in  $x$  and  $z$  directions, and lower-case letters represent the fluctuating components (e.g.,  $u = U - \langle U \rangle$ ). The superscript ‘+’ denotes quantities normalized by the inner variables of each case.

To analyse the Qs responsible for the turbulent skin friction, we identify three-dimensional clusters of intense  $uv$  in the instantaneous flow field in an analogous manner to that reported in previous work (Lozano-Durán et al., 2012). The clusters are defined as contiguous regions that satisfy

$$|-u(\mathbf{x})v(\mathbf{x})| > Hu_{rms}(y)v_{rms}(y), \quad (2)$$

where  $-u(\mathbf{x})v(\mathbf{x})$  is the instantaneous RSS,  $u_{rms}$  and  $v_{rms}$  denote the root mean square (RMS) of  $u$  and  $v$ , respectively, and  $H$  is the hyperbolic-hole size. Here, we set  $H = 1.75$ , in accordance with the work of Lozano-Durán et al. (2012), where the percolation transition occurs. According to  $H$ , the results of structure identification could be altered. However, in the vicinity of the percolation transition region, the results presented in this work remain qualitatively unchanged. When identifying the contiguous regions, we define a connectivity rule in which a node is connected to its six orthogonal neighbours similar to the previous works (del Álamo et al., 2006; Lozano-Durán et al., 2012; Hwang & Sung, 2018, 2019). The identified clusters of Qs are then classified into different quadrants (Q1–Q4) according to the signs of  $u_m$  and  $v_m$ , which are computed over the volume of each cluster ( $\Omega$ ),

$$\mathbf{u}_m = \frac{\int_{\Omega} \mathbf{u} d\Omega}{\int_{\Omega} d\Omega}. \quad (3)$$

We designate the identified clusters as Q1 structures (Q1s) if  $u_m > 0$  and  $v_m > 0$ , Q2 structures (Q2s) if  $u_m < 0$  and  $v_m > 0$ , Q3 structures (Q3s) if  $u_m < 0$  and  $v_m < 0$ , and Q4 structures (Q4s) if  $u_m > 0$  and  $v_m < 0$ . For the structures whose centers are located in the upper half of the channel, we change the sign of the corresponding  $v_m$ .

Next, we classified the extracted Qs based on their minimum wall-normal distances ( $y_{min}$ ), defining Qs as wall-attached when  $y_{min}^+ < 20$  and as wall-detached when  $y_{min}^+ > 20$  (del Álamo et al., 2006; Lozano-Durán et al., 2012). Among the extracted Qs, Q1s and Q3s (Q<sup>+</sup>s) occupied 0.1% and 0.6% of the total channel volume for attached and detached structures, respectively, while Q2s and Q4s (Q<sup>-</sup>s) comprised 6% for attached and 2% for detached structures. Consequently, our study primarily focused on wall-attached Q<sup>-</sup>s.

## RESULTS AND DISCUSSION

To examine the behaviour of wall-attached Q<sup>-</sup>s under slip conditions and the Re effect, we first explore the identified structures in an instantaneous flow field. Figure 1 displays the iso-surfaces of wall-attached Q<sup>-</sup>s. Here, we exclude the structures with a volume of less than 30<sup>3</sup> wall units (del Álamo et al., 2006; Hwang & Sung, 2018). Green and orange iso-surfaces represent Q2s and Q4s, respectively; dark-to-light shading indicates proximity to the wall. As seen, the extracted structures span over a wide range of scales, extending from the near-wall region to the outer region. Moreover, the wall-attached Q2s and Q4s are aligned side by side in the spanwise direction, indicating that most of the wall-attached Q2s and Q4s are organized in side-by-side pairs (Lozano-Durán et al., 2012). Comparing the no-slip (figure 1a,c) and slip cases (figure 1b,d), it is observed that the slip conditions lead to a reduction in the number of structures. Upon closer examination, applying the slip conditions results in an elongation of the structures in the streamwise direction and an increase in overall size. Despite the reduction in the number of structures, the total volume remains unchanged.

Upon observing the Re effect, it is evident that the multiscale phenomena become more pronounced with higher Re. Moreover, as seen in figure 1(a,c), there is an increase in both the number of structures and their occupied volume. This indicates that the importance of wall-attached structures increases with higher Re. When comparing the slip cases (figure 1b,d), it is observed that at the high Re, the reduction in the number of structures is more significant than at the low Re.

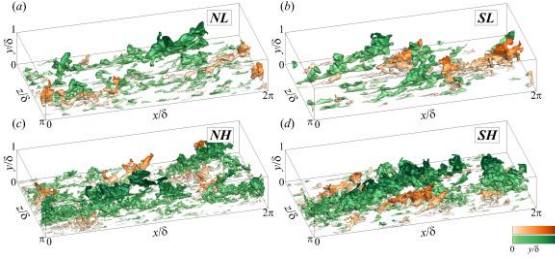


Figure 1. Identified wall-attached Q2 and Q4 structures in an instantaneous flow field: (a) NL; (b) SL; (c) NH; and (d) SH. The Q2 and Q4 structures are represented in green and orange, respectively.

As mentioned previously, the drag is reduced by 33% and 44% in the low and high Re cases, respectively. To explore the skin friction reduction due to wall-attached structures, we first decompose the skin friction coefficient ( $C_f$ ) using the FIK identity (Fukagata et al., 2002):

$$C_f = \frac{6}{Re_b} \left( 1 - \frac{\langle U_s \rangle}{U_b} \right) + \frac{6}{U_b^2} \int_0^1 \left( 1 - \frac{y}{\delta} \right) \langle -uv \rangle d \left( \frac{y}{\delta} \right). \quad (4)$$

Here, the first and second terms in the right-hand side correspond to the laminar and turbulent contributions ( $C_{f1}$  and  $C_{f2}$ ), respectively. Note that  $U_s = 0$  for the no-slip case. Since the integrand of  $C_{f2}$  contains  $\langle -uv \rangle$ , we can further decompose  $C_{f2}$  into three categories based on the identified structures: wall-attached Q<sup>-</sup>s ( $C_{fa}$ ), wall-detached Q<sup>-</sup>s ( $C_{fd}$ ), and others ( $C_{fo}$ , including Q<sup>+</sup>s and weak  $uv$  regions). Hence,  $C_{f2} = C_{fa} + C_{fd} + C_{fo}$ . The corresponding results are presented in figure 2. For both Re,  $C_{f2}$  is much larger than  $C_{f1}$ . The turbulent contribution  $C_{f2}$  comprises over 90% of  $C_f$ , whereas  $C_{f1}$  is less significant

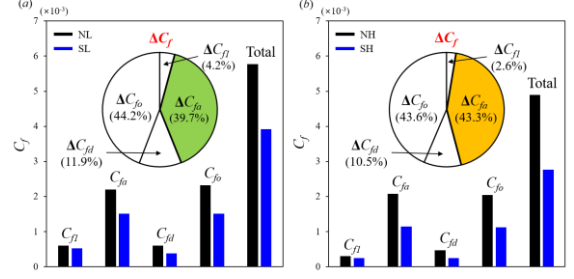


Figure 2. Decomposition of the skin-friction coefficient and the contribution to the reduced skin-friction coefficient using FIK identity: (a) low Reynolds number; (b) high Reynolds number

and diminishes with increasing Re. Notably, the wall-attached Q<sup>-</sup>s ( $C_{fa}$ ) primarily contribute to turbulent skin friction ( $C_{f2}$ ), accounting for nearly 50%, although the identified wall-attached Q<sup>-</sup>s only occupy 6% of the total volume. This observation reflects the importance of understanding wall-attached structures in exploring the mechanism of skin friction generation.

Moreover, these structures are responsible for most of the reduced  $C_f$ . This is highlighted in the pie chart in figure 2. Here, the contribution of the decomposed  $C_f$  to the total reduced  $C_f$  is calculated as the ratio of the reduced skin friction for each structure ( $\Delta C_{fi}$ ) to the total reduced skin friction ( $\Delta C_f$ ). As seen, the contribution of the wall-attached Q<sup>-</sup>s to  $\Delta C_f$  accounts for approximately 40%. Notably, with an increase in the Re, it is particularly the wall-attached structures whose contribution increases, in contrast to the wall-detached and other structures, which see a decrease in their contributions. This result suggests that wall-attached structures are responsible for the reduction of turbulent skin friction, a role that becomes increasingly significant with higher Re. This could be due to the fact that these structures exist over a wide range of scales and extend from the near-wall region to the outer region (figure 1). Hence, understanding their contribution to turbulent skin friction is essential. We will focus on analysing the contribution of wall-attached structures with respect to their height ( $l_y$ ).

Figure 3 illustrates the mean length ( $\langle l_x \rangle$ ) and width ( $\langle l_z \rangle$ ) of wall-attached Q<sup>-</sup>s with respect to  $l_y$ , where  $l_x$  and  $l_z$  are the streamwise and spanwise lengths of each structure correspond to the wall-parallel sizes of the bounding box for each structure. The blue and black circle symbols represent slip and no-slip cases, respectively. Although there are some deviations in the  $\langle l_x \rangle$  between the slip and no-slip cases (figure 3a,b), the variations of the  $\langle l_z \rangle$  collapse well regardless of the boundary conditions over a broad range (figure 3b,d), indicating that streamwise slip does not alter the  $\langle l_z^+ \rangle$ . Furthermore,  $\langle l_z \rangle$  exhibits a linear relationship with  $l_y$  at both Re in the region  $3Re\tau^{0.5} < l_y^+$  (indicated by red lines). Here,  $3Re\tau^{0.5}$  denotes the limit of the logarithmic region (Marusic et al., 2013). Conversely, in figure 3(a,c),  $\langle l_x \rangle$  within the range  $3Re\tau^{0.5} < l_y^+ < 0.6\delta^+$  shows a power-law behaviour (denoted by red lines). The power-law behaviour ( $\langle l_x \rangle \sim l_y^{0.74}$ ) slightly differs from the linear relationship ( $\langle l_x \rangle \sim l_y$ ) suggested by a previous work (Lozano-Durán et al., 2012). This discrepancy may be attributed to the lower Re in our study. Beyond  $l_y^+ = 0.6\delta^+$ ,  $\langle l_x \rangle$  deviates from the power-law behaviour. Based on these characteristics, we classify the wall-attached Q<sup>-</sup>s into three groups based on  $l_y$  similar to the classification by Hwang et al. (2020): buffer-layer structure (WAB) for  $l_y^+ < 3Re\tau^{0.5}$ ; self-

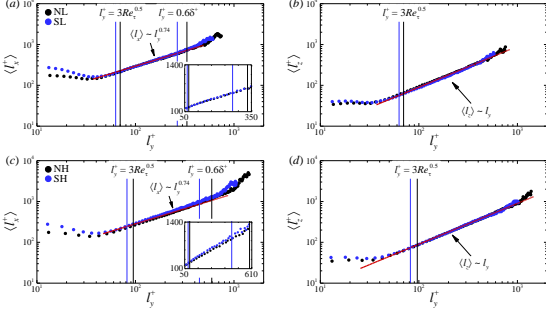


Figure 3. Mean length ( $\langle l_x \rangle$ ) and width ( $\langle l_z \rangle$ ) of wall-attached Q's with respect to their wall-normal height ( $l_y$ ). The blue and black circles correspond to the slip and no-slip cases, respectively. In (a,c), the red lines represent  $\langle l_x \rangle \sim l_y^{0.74}$  and the vertical lines indicate  $l_y^+ = 3Re_\tau^{0.5}$  and  $0.6\delta^+$  for each case. The insets show the linear-linear plot where  $3Re_\tau^{0.5} < l_y^+ < 0.6\delta^+$ . In (b,d), the red lines correspond to  $\langle l_x \rangle \sim l_y$ .

similar structure (WASS) for  $3Re_\tau^{0.5} < l_y^+ < 0.6\delta^+$ ; non-self-similar structure (WANS) for  $0.6\delta^+ < l_y^+$ .

Investigating the variations in the size of classified structures under slip conditions, the WAB experience an elongation in  $\langle l_x^+ \rangle$  at both Re, particularly for those with  $l_y^+ < 40$ , as shown in figure 3(a,c). For the WASS, a slight discrepancy in  $\langle l_x^+ \rangle$  between NH and SH is observed. To further explore this observation, the linear-linear plots of  $\langle l_x^+ \rangle$  and  $l_y^+$  for the WASS are presented in the insets. At the low Re,  $\langle l_x^+ \rangle$  remains consistent for a given  $l_y^+$  regardless of the boundary conditions, indicating that the self-similarity is sustained under slip conditions. This aligns with a previous study (Yoon & Sung, 2022) suggesting that the impact of streamwise slip on wall-attached  $u$  structures is confined below the logarithmic region. However, while self-similarity is preserved under slip conditions at the high Re, there is a noticeable increase in  $\langle l_x^+ \rangle$ . This implies that the effects of streamwise slip extend beyond the near-wall region into the logarithmic region. For the WANS, the similar behaviours appear under slip conditions compared to no-slip cases.

To assess the impact of the classified structures (WAB, WASS, and WANS) on the drag reduction across different Re, the contribution of each classified structure to skin-friction reduction is investigated. Figure 4 presents pie charts illustrating how each classified structure contributes to the skin-friction reduction. The contributions of the WANS and WASS are notably significant, accounting for nearly 60% and 30%, respectively. Considering that the WANS occupies 5% of the total channel volume and the WASS only 1%, it highlights the crucial role of the WASS in reducing skin friction. Meanwhile, as the Re increases, the contribution of the WANS

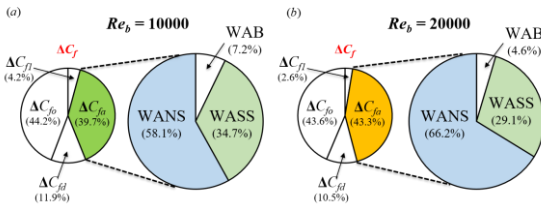


Figure 4. Contribution of the classified structures to skin-friction reduction induced by wall-attached Q's: (a) low Reynolds number; (b) high Reynolds number

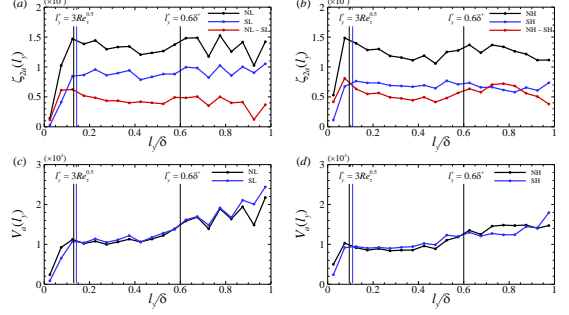


Figure 5. Histograms of  $\zeta_{2a}$  and  $V_a$  with respect to  $l_y$ : (a,c) low Reynolds number; (b,d) high Reynolds number. 20 bins are used while varying  $l_y$  from 0 to  $1.0\delta$ . The blue and black lines denote the slip and no-slip cases, respectively. In panels (a) and (b), the red lines indicate the difference between no-slip and slip cases for the same  $l_y$ .

to skin-friction reduction grows, while the contributions from other structures diminish.

After examining the skin-friction reduction contributed by each classified structure, we become curious whether skin-friction reduction predominantly occurs at a particular  $l_y$ . This leads us to explore the skin-friction reduction and volume of these structures with respect to their  $l_y$ . Figure 5 displays histograms representing the skin-friction contribution and the volumes of wall-attached Q's normalized by the channel volume across  $l_y$  for each case. Here,  $\zeta_{2a}$  and  $V_a$  are defined as:

$$\zeta_{2a}(l_y) = \frac{\frac{1}{L_x L_z} \left\langle \frac{6}{U_b^2} \int_{\Omega_{l_y}} - \left(1 - \frac{y}{\delta}\right) u(x)v(x) d\Omega \right\rangle}{(C_f)_N}, \quad (5)$$

$$V_a(l_y) = \frac{1}{L_x L_y L_z} \left\langle \int_{\Omega_{l_y}} d\Omega \right\rangle, \quad (6)$$

where  $(C_f)_N$  represents the  $C_f$  for the no-slip cases. We focus on WASS and WANS, which make a dominant contribution to skin-friction reduction. For the WASS ( $3Re_\tau^{0.5} < l_y^+ < 0.6\delta^+$ ), there is no dominant  $l_y$  for skin-friction reduction. However, for structures within  $0.2\delta < l_y < 0.5\delta$ , a nearly identical skin-friction reduction (indicated by the red lines) occurs as seen in figure 5(a,b). Interestingly, in figure 5(c,d), the volume of these structures is nearly uniform regardless of their  $l_y$ . Moreover, applying slip conditions does not alter the volume at the same  $l_y$ , compared to the no-slip case. These features prompt us to conduct further analysis from the perspective of the RSS carried by WASS (discussed in detail in figure 6). For the WANS ( $0.6\delta^+ < l_y^+$ ), differences between the two Re can be observed. When looking at structures within the range  $0.7\delta < l_y < 0.9\delta$ , SL shows a larger volume compared to NL, whereas the volume is reduced in SH when compared to NH. As a result, we can see that the structures in that range contribute to a greater skin-friction reduction at the high Re than low Re.

Next, we conditionally average the RSS ( $\langle RSS_a^*(y, l_y) \rangle$ ) with respect to  $l_y$  to examine the RSS carried by wall-attached structures across their heights, similar to previous works (Hwang & Sung 2018; Hwang & Sung 2019):

$$\langle RSS_a^* \rangle(y, l_y) = \left\langle \frac{1}{S_a(y, l_y)} \int_{S_a} -u(x)v(x) dx dz \right\rangle, \quad (7)$$

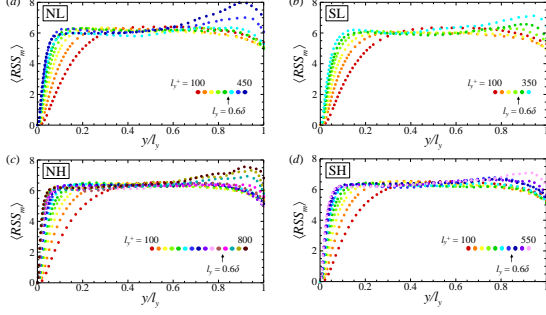


Figure 6. The profiles of  $\langle RSS_m \rangle$  for various  $l_y$ : (a) NL, (b) SL, (c) NH, and (d) SH. The color symbols represent different  $l_y^+$  values, with each color increment corresponding to  $50\nu/u_\tau$ .

where  $S_a$  is the wall-parallel area of each structure at  $y$ . We find that the RSS in the upper part of each structure is inversely proportional to  $y$  for relatively tall attached structures that extend beyond the logarithmic region. This observation is reminiscent of the wall-normal distribution of the total shear stress in fully-developed internal flows. Given this finding, we normalize  $\langle RSS_a^*(y, l_y) \rangle$  by the total shear stress:

$$\langle RSS_m \rangle(y, l_y) = \frac{\langle RSS_a^* \rangle}{\frac{\langle \tau_w \rangle}{\rho} \left(1 - \frac{y}{\delta}\right)} = \frac{\langle RSS_a^* \rangle}{u_\tau^2 \left(1 - \frac{y}{\delta}\right)}, \quad (8)$$

where  $\rho$  and  $\langle \tau_w \rangle$  are the fluid density and the wall-shear stress, respectively. As shown in Eq. (8),  $\langle RSS_m \rangle$  also can be considered as  $\langle RSS_a^* \rangle$  scaled by the square of the characteristic velocity scale (i.e.,  $u_\tau(1-y/\delta)^{1/2}$ ), which corresponds to the velocity scale of attached eddies proposed by Lozano-Durán & Bae (2019).

Figure 6 shows  $\langle RSS_m \rangle$  profiles for various  $l_y$  values in each case. Here, the wall-normal distance is normalized by  $l_y$ . For the structures with  $200 \leq l_y^+ < 0.6\delta^+$ , the scaled profiles are in good agreement within regions where  $y/l_y > 0.2$ , regardless of boundary conditions and Re. Notably,  $\langle RSS_m \rangle$  is consistently equal to 6 in that region, indicating that the  $\rho \langle RSS_a^* \rangle$  of these structures is six times the total shear stress at a given  $y$ . In contrast, for structures with  $0.6\delta^+ < l_y^+$  (corresponding to the WANS),  $\langle RSS_m \rangle$  deviates from 6 in regions where  $y/l_y > 0.6$ . Consequently, we confirm the self-similar behaviour of the RSS carried by the WASS. Given this fact, we can predict the amount of the skin-friction reduction carried by WASS.

As observed in figure 4, the contribution of the WANS to the skin-friction reduction increases with higher Re. Moreover, as seen in figure 5, we find that the change in the volume of WANS at specific  $l_y$  under slip conditions varies with Re. To further explore how slip conditions affect the momentum transfer within the WANS, we compute the conditional two-point correlation of the wall-normal velocity fluctuations within WANS. The conditional correlation coefficient ( $R$ ) is defined as follows:

$$R[v_{NS}, v_{NS}](r_x, y, r_z; y_{ref}) = \frac{\langle v_{NS}(x, z; y_{ref})v_{NS}(x+r_x, y, z+r_z) \rangle}{\sigma_v(y_{ref})\sigma_v(y)}, \quad (9)$$

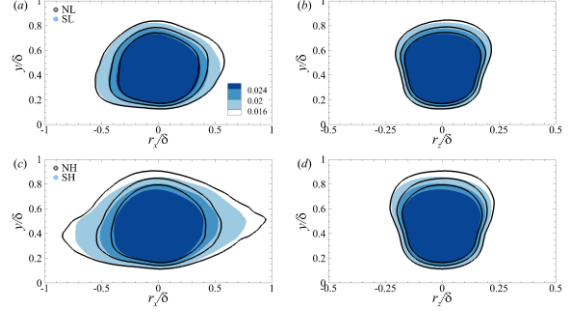


Figure 7. Conditional correlations of wall-normal velocity fluctuations for WANS, (a,c) in the  $x$ - $y$  plane ( $r_z/\delta = 0$ ) and (b,d) in the  $y$ - $z$  plane ( $r_x/\delta = 0$ ): (a,b) low Reynolds number; (c,d) high Reynolds number. The color and black line contours correspond to the slip and no-slip cases, respectively.

where  $\sigma_v$  and  $v_{NS}$  represent the RMS of  $v$  and the conditionally sampled  $v$  within WANS, respectively. Figure 7 shows the  $x$ - $y$  and  $y$ - $z$  planes of the conditional correlations at  $y_{ref} = 0.4\delta$ . In figure 7(a,b), the contours collapse well for both NL and SL, indicating that the average extent of the wall-normal momentum transport within the WANS remains consistent under slip conditions at the low Re. Conversely, as seen in figure 7(c,d), the contours of SH and NH do not collapse with each other, indicating that the extent of the wall-normal transport carried by WANS is reduced in SH. This decrease in the WANS appears to affect the skin-friction reduction, suggesting that the contribution of the WANS to skin-friction reduction amplifies with increasing Re. Given that these structures extend across the outer region, especially the core region of internal flows (Yang et al., 2016, 2019), we will further analyse their dynamics in future efforts.

## CONCLUSIONS

We explore the reduction in turbulent skin friction in slip channel flows at  $Re_b = 10,000$  and  $20,000$ . Extracting the wall-attached Q2 and Q4 structures (Q<sup>-</sup>s) from the DNS data, we assess their contribution to turbulent skin friction using the FIK identity (Fukagata et al., 2002). Wall-attached Q<sup>-</sup>s account for more than 50% of turbulent skin friction generation and nearly 40% of skin-friction reduction, despite occupying only 6% of the total domain volume. Furthermore, the importance of wall-attached Q<sup>-</sup>s increases with increasing Re. We classify the wall-attached Q<sup>-</sup>s as buffer-layer (WAB), self-similar (WASS), and non-self-similar (WANS) structures with respect to their height ( $l_y$ ). Among these, the WASS and WANS are dominant in skin-friction reduction. For the WASS ( $3Re_\tau^{0.5} < l_y^+ < 0.6\delta^+$ ), their volume remains unchanged across  $l_y$  in both slip and no-slip cases. Moreover, the contribution of WASS to the skin-friction reduction also remains unchanged, confirming that the RSS carried by the WASS exhibit self-similarity. For the WANS ( $0.6\delta^+ < l_y^+$ ), their contribution to the skin-friction reduction grows with increasing Re. Through conditional two-point correlation analysis, we observe that the decrease in the average extent of the wall-normal transport by WANS under slip conditions especially at high Re. This decrease appears to contribute to a larger amount of skin-friction reduction at the high Re compare to low Re. Our results enhance the understanding of the behaviour of wall-attached self-similar and non-self-similar structures in drag-reduced flows and

potentially contribute to developing new drag reduction methods by manipulating those structures.

## ACKNOWLEDGEMENTS

This work was supported by a National Research Foundation of Korea (NRF) grant funded by the Korea government (MSIT) (Grant No. RS-2023-00211896).

## REFERENCES

- Adrian, R. J., 2007, "Hairpin vortex organization in wall turbulence", *Physics of Fluids* Vol. 19.
- de Giovanetti, M., Hwang, Y., & Choi, H., 2016, "Skin-friction generation by attached eddies in turbulent channel flow", *Journal of Fluid Mechanics* Vol. 808, pp. 511-538.
- del Álamo, J. C., Jiménez, J., Zandonade, P., & Moser, R. D., 2006, "Self-similar vortex clusters in the turbulent logarithmic region", *Journal of Fluid Mechanics* Vol. 561, pp. 329-358.
- Fukagata, K., Iwamoto, K., & Kasagi, N., 2002, "Contribution of Reynolds stress distribution to the skin friction in wall-bounded flows", *Physics of Fluids* Vol. 14, pp. L73-L76.
- Hamilton, J. M., Kim, J., & Waleffe, F., 1995, "Regeneration mechanisms of near-wall turbulence structures", *Journal of Fluid Mechanics* Vol. 287, pp. 317-348.
- Han, J., Hwang, J., Yoon, M., Ahn, J., & Sung, H. J., 2019, "Azimuthal organization of large-scale motions in a turbulent minimal pipe flow", *Physics of Fluids* Vol. 31.
- Hutchins, N., & Marusic, I., 2007, "Large-scale influences in near-wall turbulence", *Philosophical Transactions of the Royal Society A: Mathematical, Physical and Engineering Sciences* Vol. 365, pp. 647-664.
- Hwang, J., Lee, J., & Sung, H. J., 2016a, "Influence of large-scale accelerating motions on turbulent pipe and channel flows", *Journal of Fluid Mechanics* Vol. 804, pp. 420-441.
- Hwang, J., Lee, J., Sung, H. J., & Zaki, T. A., 2016b, "Inner-outer interactions of large-scale structures in turbulent channel flow", *Journal of Fluid Mechanics* Vol. 790, pp. 128-157.
- Hwang, J., & Lee, J. H., 2022, "Meandering features of wall-attached structures in turbulent boundary layer", *Physical Review Fluids* Vol. 7, pp. 114603.
- Hwang, J., Lee, J. H., & Sung, H. J., 2020, "Statistical behaviour of self-similar structures in canonical wall turbulence", *Journal of Fluid Mechanics* Vol. 905, pp. A6.
- Hwang, J., & Sung, H. J., 2017, "Influence of large-scale motions on the frictional drag in a turbulent boundary layer", *Journal of Fluid Mechanics* Vol. 829, pp. 751-779.
- Hwang, J., & Sung, H. J., 2018, "Wall-attached structures of velocity fluctuations in a turbulent boundary layer", *Journal of Fluid Mechanics* Vol. 856, pp. 958-983.
- Hwang, J., & Sung, H. J., 2019, "Wall-attached clusters for the logarithmic velocity law in turbulent pipe flow", *Physics of Fluids* Vol. 31.
- Kasagi, N., Suzuki, Y., & Fukagata, K., 2009, "Microelectromechanical systems-based feedback control of turbulence for skin friction reduction", *Annual review of fluid mechanics* Vol. 41, pp. 231-251.
- Kim, J., 2011, "Physics and control of wall turbulence for drag reduction", *Philosophical Transactions of the Royal Society A: Mathematical, Physical and Engineering Sciences* Vol. 369, pp. 1396-1411.
- Kim, K., Baek, S. J., & Sung, H. J., 2002, "An implicit velocity decoupling procedure for the incompressible Navier-Stokes equations", *International journal for numerical methods in fluids* Vol. 38, pp. 125-138.
- Kim, K. C., & Adrian, R. J., 1999, "Very large-scale motion in the outer layer", *Physics of Fluids* Vol. 11, pp. 417-422.
- Kline, S. J., Reynolds, W. C., Schraub, F., & Runstadler, P., 1967, "The structure of turbulent boundary layers", *Journal of Fluid Mechanics* Vol. 30, pp. 741-773.
- Kovaszny, L. S., Kibens, V., & Blackwelder, R. F., 1970, "Large-scale motion in the intermittent region of a turbulent boundary layer", *Journal of Fluid Mechanics* Vol. 41, pp. 283-325.
- Lozano-Durán, A., & Bae, H. J., 2019, "Characteristic scales of Townsend's wall-attached eddies", *Journal of Fluid Mechanics* Vol. 868, pp. 698-725.
- Lozano-Durán, A., Flores, O., & Jiménez, J., 2012, "The three-dimensional structure of momentum transfer in turbulent channels", *Journal of Fluid Mechanics* Vol. 694, pp. 100-130.
- Lozano-Durán, A., & Jiménez, J., 2014, "Effect of the computational domain on direct simulations of turbulent channels up to  $Re\tau = 4200$ ", *Physics of Fluids* Vol. 26.
- Lu, S., & Willmarth, W., 1973, "Measurements of the structure of the Reynolds stress in a turbulent boundary layer", *Journal of Fluid Mechanics* Vol. 60, pp. 481-511.
- Marusic, I., Monty, J. P., Hultmark, M., & Smits, A. J., 2013, "On the logarithmic region in wall turbulence", *Journal of Fluid Mechanics* Vol. 716, pp. R3.
- Min, T., & Kim, J., 2004, "Effects of hydrophobic surface on skin-friction drag", *Physics of Fluids* Vol. 16, pp. L55-L58.
- Robinson, S. K., 1991, "Coherent motions in the turbulent boundary layer", *Annual review of fluid mechanics* Vol. 23, pp. 601-639.
- Townsend, A., 1961, "Equilibrium layers and wall turbulence", *Journal of Fluid Mechanics* Vol. 11, pp. 97-120.
- Tretheway, D. C., & Meinhart, C. D., 2002, "Apparent fluid slip at hydrophobic microchannel walls", *Physics of Fluids* Vol. 14, pp. L9-L12.
- Wallace, J. M., Eckelmann, H., & Brodkey, R. S., 1972, "The wall region in turbulent shear flow", *Journal of Fluid Mechanics* Vol. 54, pp. 39-48.
- Willmarth, W., & Lu, S., 1972, "Structure of the Reynolds stress near the wall", *Journal of Fluid Mechanics* Vol. 55, pp. 65-92.
- Yang, J., Hwang, J., & Sung, H. J., 2016, "Structural organization of the quiescent core region in a turbulent channel flow", *International Journal of Heat and Fluid Flow* Vol. 62, pp. 455-463.
- Yang, J., Hwang, J., & Sung, H. J., 2019, "Influence of wall-attached structures on the boundary of the quiescent core region in turbulent pipe flow", *Physical Review Fluids* Vol. 4, pp. 114606.
- Yoon, M., Ahn, J., Hwang, J., & Sung, H. J., 2016a, "Contribution of velocity-vorticity correlations to the frictional drag in wall-bounded turbulent flows", *Physics of Fluids* Vol. 28.
- Yoon, M., Hwang, J., Lee, J., Sung, H. J., & Kim, J., 2016b, "Large-scale motions in a turbulent channel flow with the slip boundary condition", *International Journal of Heat and Fluid Flow* Vol. 61, pp. 96-107.
- Yoon, M., Hwang, J., & Sung, H. J., 2018, "Contribution of large-scale motions to the skin friction in a moderate adverse pressure gradient turbulent boundary layer", *Journal of Fluid Mechanics* Vol. 848, pp. 288-311.
- Yoon, M., & Sung, H. J., 2022, "Wall-attached structures in a drag-reduced turbulent channel flow", *Journal of Fluid Mechanics* Vol. 943, pp. A14.